DOI: 10.1002/chem.200700339

Nanofibers of Fullerene C_{60} through Interplay of Ball-and-Socket Supermolecules

Lee J. Hubble[b] and Colin L. Raston*[a]

Abstract: Mixing solutions of *p*-*t*Bu-calix[5]arene and C_{60} in toluene results in a 1:1 complex $(C_{60})\cap$(*p*-*t*Bu-calix[5]-arene), which precipitates as nanofibers. The principle structural unit is based on a host–guest ball-and-socket nanostructure of the two components, with an extended structure comprising zigzag/helical arrays of fullerenes (powder X-ray diffraction data coupled with molecular modeling). Under argon at temperatures above 309 °C, the fibers undergo selective volatilization of the calixarenes to afford C_{60}-core nanostructures encapsulated in a graphitic material sheath, which exhibits a dramatic increase in surface area. Above 650 °C the material exhibits an ohmic conductance response, due to the encapsulation process.

Keywords: calixarenes · fullerenes · host–guest systems · nanostructures · supramolecular chemistry

Introduction

Carbon-based materials have a wide variety of applications such as catalysis,[1–4] fuel cells,[5–7] separations,[8–11] extractions, and sensor technology.[12–14] Overall, carbon is remarkably versatile and offers the possibility of fabricating a diverse range of novel products entirely composed of the element. The discovery of fullerene C_{60} and higher fullerenes, and the later development of carbon nanotubes, has added significantly to this possibility becoming a reality.

In developing the full potential of carbon it is important to be able to accurately prepare new structural carbon frameworks and to be able to generate new materials with different spatial arrangement of arrays of carbon atoms. One way of achieving this is through self-assembly processes. Fullerenes, as the only form of molecular carbon, are in a unique position to be used for these processes. A recent example of this is the formation of a one-dimensional C_{60} array in solution templated by helical nanotubes[15]

An area that has attracted significant attention in recent years is the supramolecular chemistry of fullerenes involving cavitands, with particular interest being devoted to calixarenes and related molecules. Atwood et al.[16] and Suzuki et al.[17] initially developed a convenient and efficient purification method for obtaining C_{60} from "crude" fullerene soot, which is based on the formation of a discrete complex with *p*-*t*Bu-calix[8]arene. Furthermore, the different effects of lower phenolic oligomers and substituted lower and upper ring functionalization has led to unique complex arrays of fullerenes that display fullerene···fullerene interplay.[18–20] Examples of such interplay include the 1:1 complexes between C_{60} and cyclotriveratrylene (CTV),[21] and calix[5]arene[22] where the C_{60} molecules are packed into continuous zigzag chains; $C_{60}\cdots C_{60}$ close contacts vary from 9.90 to 10.20 Å, with dihedral angles in the chains ranging from 118 to 172°, indicating a transitional packing structure between a linear chain and double-column array.[20]

Bowl-shaped calix[5]arenes are effective in controlling the assembly of fullerenes, with dimensionality and curvature complementarity for *endo*-cavity binding C_{60}.[23] Herein we show that *p*-*t*Bu-calix[5]arene forms a complex with C_{60} from toluene, as nanofibers based on the 1:1 supermolecule $(C_{60})\cap$(*p*-*t*Bu-calix[5]arene) [Eq. (1)].

Optical and transmission electron micrographs of the structure of these bundles of nanofibers are presented in Figure 1a and 1b, respectively. We also show that the calixarenes can be removed at high temperatures under an inert atmosphere to afford encapsulated nanofibers of pure C_{60} with a large increase in surface area compared to the parent complex. Furthermore, we indicate that "crude" fullerene soot similarly affords nanofibers, albeit with a small percent-

[a] Prof. C. L. Raston
School of Biomedical, Biomolecular & Chemical Sciences
University of Western Australia
35 Stirling Highway, Crawley, 6009 (Australia)
Fax: (+61) 8-6488-8683
E-mail: clraston@chem.uwa.edu.au

[b] L. J. Hubble
Centre for Forensic Science, University of Western Australia
35 Stirling Highway, Crawley, 6009 (Australia)

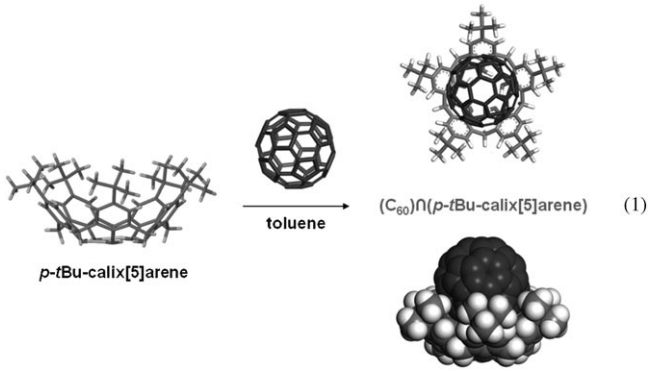

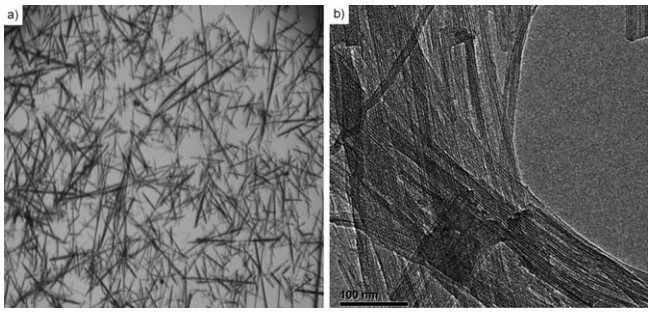

Figure 1. Optical micrograph (a) and TEM image (b) of the $(C_{60})\cap$(*p*-*t*Bu-calix[5]arene) complex, the latter revealing the linear striations of fullerene C_{60} within bundles of nanofibers.

age of the next highest fullerene, C_{70}, incorporated into the structure.

Results and Discussion

The synthesis of the $(C_{60})\cap$(*p*-*t*Bu-calix[5]arene) complex requires a large excess of calixarene, and is formed in 56% yield based on C_{60}. After two hours the typical magenta color of the C_{60} solution turns dark brown indicating complex formation. At this point optical microscopy reveals a suspension of light brown needlelike, fibrous material (Figure 1a). To ensure a uniform product, continuous stirring is essential. The mother liquor can be recycled with the addition of an equivalent of C_{60} and *p*-*t*Bu-calix[5]arene, thereafter affording a quantitative yield of the complex. A variety of different synthetic and crystallization conditions were investigated, such as different host–guest molar ratios, host–guest reaction periods, rates of solvent evaporation, solventless reactions, and the use of ultrasonication. Indeed, grinding an equimolar mixture of C_{60} and *p*-*t*Bu-calix[5]arene followed by sonication in hexane afforded the same fibrous product, albeit in low purity with un-reacted starting material present.

Using a mixture of fullerenes (fullerite) in place of C_{60} also afforded a nanofiber complex, with some C_{70} incorporated (UV/Vis), whereas reacting pure C_{70} with the same calixarene did not form a solid complex. The structure of the complex derived from fullerite is presumably the same as the structure for the complex formed by using pure C_{60} (see below), with the upper limit of C_{70} inclusion governed by the geometrical mismatch associated with incorporating a non-spheroidal fullerene into the continuous array. The $(C_{60})\cap$(*p*-*t*Bu-calix[5]arene) complex undergoes rapid decomposition in dichloromethane, with the precipitation of pure C_{60} (Figure 2). The analogous $(C_{60})\cap$(*p*-*t*Bu-calix[8]arene) complex similarly degrades in dichloromethane.[16]

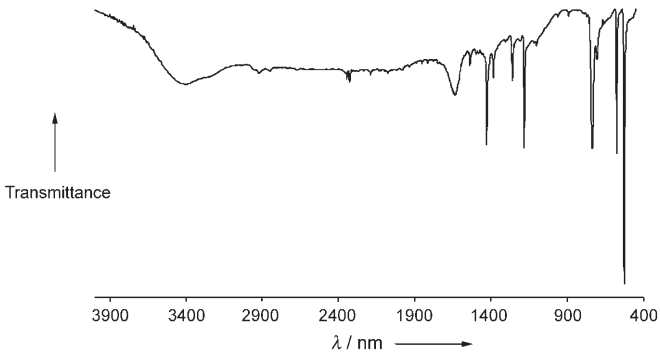

Figure 2. IR spectra of the product of the decomplexation of $(C_{60})\cap$(*p*-*t*Bu-calix[5]arene) in dichloromethane, additional absorbance peaks are attributed to residual dichloromethane.[16]

Solid-state NMR spectroscopy of the complex clearly shows freely rotating C_{60} at ambient temperature, and also some rotation of the tertiary butyl groups (Figure 3). The

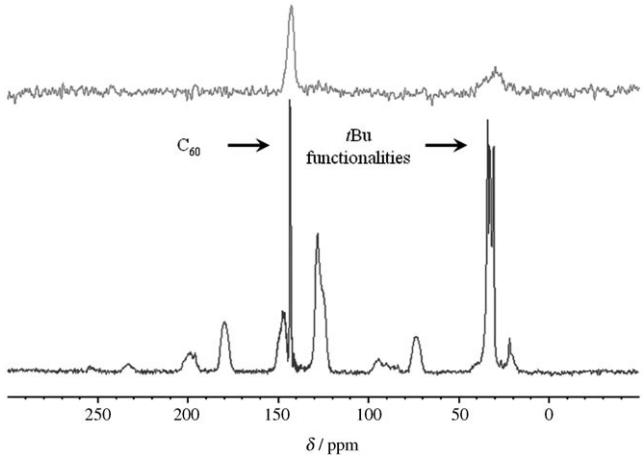

Figure 3. CP-MAS solid state ^{13}C NMR spectra for $(C_{60})\cap$(*p*-*t*Bu-calix[5]arene), with (bottom) and without (top) magic angle spinning.

TEM image shows ordered linear striations throughout the nanofibers, which correlate to columnar arrays of fullerenes (see Figure 1b).

Calix[5]arenes have complementarity of curvature with C_{60} and form complexes with the fullerene residing in the cavity, either as a ball-and-socket nanostructure, or with two calixarenes shrouding a single fullerene molecule.[22,24] This,

coupled with the ratio of 1:1 for the two components in the present complex, is consistent with the supermolecule unit as a ball-and-socket nanostructure [Eq. (1)]. The supermolecules then propagate to 1D arrays, attributed to columnar arrays of C_{60}, noting that such an array is encountered in the calix[5]arene system.[22] Bundles of these arrays agglomerate to form the macroscopic fibrous product. In comparison to the calix[5]arene system, the present system has additional geometrical packing constraints due to the bulky tertiary butyl groups on the upper rim of the calixarene, but nevertheless fullerene···fullerene interactions are still possible.

The powder X-ray diffraction (PXRD) pattern is dominated by a 2θ peak at 3.93° (Figure 4), which is attributed to the inherent distance between individual C_{60} columns, at a

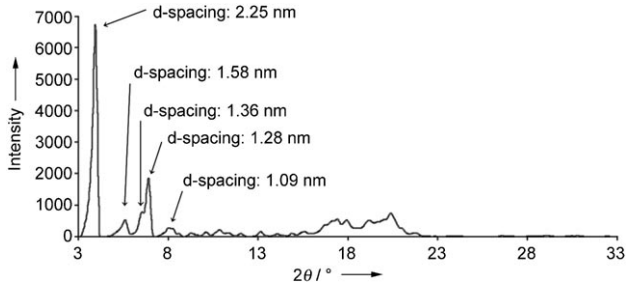

Figure 4. Powder X-ray diffraction pattern of $(C_{60})\cap$(*p*-*t*Bu-calix[5]arene).

distance of 2.25 nm. The fibrous nature of the sample gives rise to preferred diffraction pattern orientation effects in the patterns at different sample orientations. The next highest intensity peak is at a 2θ value of 6.89° with a d-spacing of 1.28 nm. Overall, the diffraction pattern and orientation effects correlate well to the proposed structure (Figure 5). Through acquisitions at different sample holder orientations

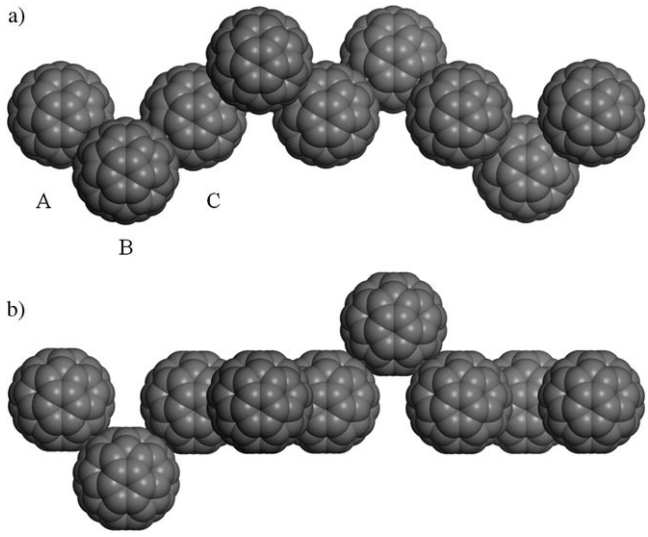

Figure 5. a) Proposed helical array of C_{60} columns; labels denote a triangular set of fullerenes. b) C_{60} column rotated 45° about the horizontal *x* axis in (a).

an increase in peak intensity at a 2θ value of 6.89° was observed. This corresponds to the three planar C_{60} molecules (A, B, & C) being parallel with the X-ray beam (Figure 5). The additional reflections correlate to other intra-column fullerene planes, with increasing angle reflections from intra-fullerene domains.

Owing to the nature of the sample, single-crystal diffraction data could not be obtained; however, the PXRD results were incorporated into a model developed by using Accelrys software.[25] For illustrative clarity, all the *p*-*t*Bu-calix[5]arene molecules shrouding the fullerenes have been omitted for Figure 5a and 5b. The model consistent with the data has a single column of C_{60} comprising three C_{60} molecules in-plane (A, B, & C) with a dihedral angle of 80.7° and centroid···centroid distances of 0.99 nm (A & B) and 1.28 nm (A & C). This is the repeating unit and is successfully rotated by 90° with four turns corresponding to a complete turn for a helical array. Atwood et al.[22] report a similar model based on single-crystal diffraction data with the unsubstituted calix[5]arene, which forms a linear zigzag array; however, this model does not fit the data obtained from PXRD in relation to the $(C_{60})\cap$(*p*-*t*Bu-calix[5]arene) complex. The arrangement of calixarenes in a single helical array is illustrated in Figure 6. This array propagates along its principle axis to form the strands of fullerene fibers seen in Figure 1b.

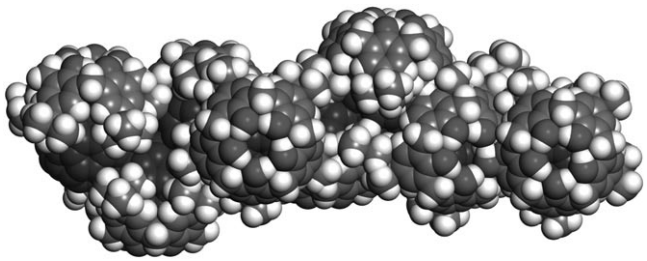

Figure 6. Proposed calixarene packing arrangement around a C_{60} column, with the same orientation as Figure 5b, based on Accelrys.[25]

Thermogravimetric analysis (TGA) studies were carried out under air and argon (Figure 7). Under air there is an initial 3% weight decrease from 23 °C until 213 °C, which is attributed to solvent surface desorption. This is interestingly

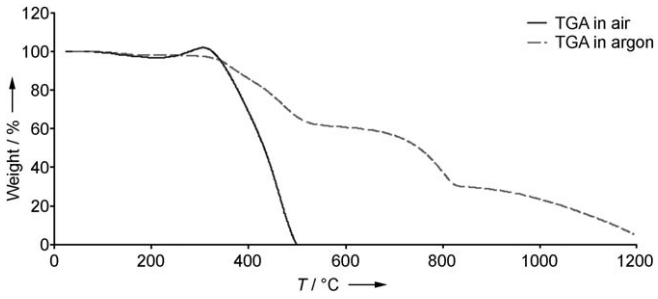

Figure 7. TGA of the nanofibers of $(C_{60})\cap$(*p*-*t*Bu-calix[5]arene) under both air and argon atmospheres.

followed by a gradual 5% weight increase from 213°C to a maximum at 309°C which is attributed to partial oxidation of C_{60}[26] followed by a gradual weight reduction at a rate of 0.6 weight% °C^{-1}, until final product decomposition at 503°C. Under argon there is an initial 2% weight loss up to 213°C followed by a 34% weight decrease from 309–517°C, then a slow declining plateau region from 517–705°C corresponding to an 8% weight loss. The total weight loss prior to C_{60} degradation corresponds to loss of the calixarene for a 1:1 complex. Further weight loss is associated with degradation of C_{60} (see below) with a change in rate of vaporization above 800°C, as reported previously by Malhotra, et al. Here there is a thermally activated transformation of the fullerenes, in which larger covalently bonded fullerene arrays are formed.[27] In the present study only 5% of the original sample weight is retained at temperatures up to 1200°C under an argon atmosphere.

Decomposition under argon was further investigated through a series of isothermal hold experiments, ranging from 400–800°C in 50°C intervals. The post-heat treated sample morphology was evaluated by using scanning electron microscopy (SEM), highlighted in Figure 8a-d. The resulting materials appear to have crystalline and amorphous domains, with PXRD results confirming crystallinity in the samples. At temperatures below 600°C the principle topographical structure was retained for bundles of nanofibers. The samples derived at 400°C were constantly plagued by charging effects, as was the case for the as-synthesized complex (Figure 8b and 8a, respectively). At annealing temperatures inclusive of 650–700°C, samples no longer suffered from charging (Figure 8c). This relates to loss of the calixarenes and also indicates that the sample is now conductive. Above 700°C structural degradation of the bundles of fullerene fibers occurs with increased surface defects, notably with pitted or 'skeleton' array structures (Figure 8d). The conductivity is associated with formation of graphitic material (see below). The degradation at high temperature aside, the selective removal of large cavitand molecules at high temperatures is without precedent in relation to fullerene architecture.

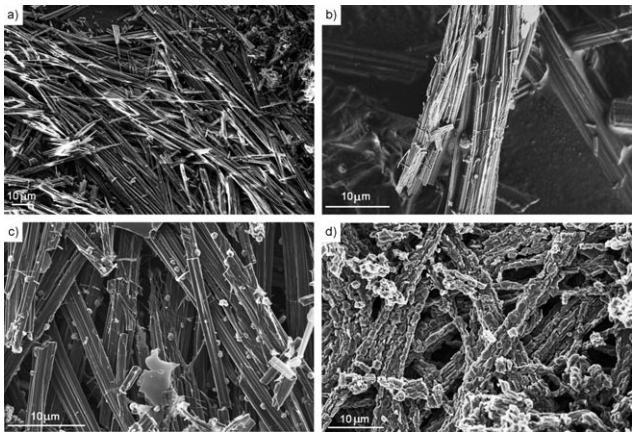

Figure 8. a) SEM image of as-synthesized bundles of nanofibers, and SEM images of bundles of nanofibers treated under argon at b) 400°C, c) 700°C, and d) 800°C, all scale bars represent 10 μm.

TGA data from the isothermal hold experiments indicate that temperatures of 650°C and 700°C, correlate to a 36 and 37% weight loss, respectively. For temperatures of 750°C and 800°C there is a 54% and 56% sample weight loss, respectively. Coupling of the SEM and TGA results suggest that heating under argon at increasing temperatures correlates to the *p*-*t*Bu-calix[5]arene backbone being selectively volatilized from the sample, leaving bundles of C_{60} nanoarrays, albeit with some graphitic material on the surface of the fibers. The formation of an all-C_{60} core structure was also confirmed by infrared spectroscopy, with typical C_{60} absorbance peaks at 526, 575, 1181 and 1428 cm^{-1}. Furthermore, PXRD on a 700°C treated sample revealed a face-centered cubic (fcc) crystal packing structure, which is the structure of pristine C_{60}.[20]

Brunauer, Emmett, and Teller (BET) surface area measurements were undertaken for the as-synthesized and isothermal hold products (Figure 9). Interestingly, there is a 45-fold increase in the surface area exhibited for the product obtained at 800°C in relation to the as-synthesized product. The surface area correlates with trends derived from TGA data (Figure 7). This indicates a steep increase in surface area until a plateau is reached at 600–700°C followed by another steep increase. The surface area increase is due to the selective volatilization of the calixarene backbone and the formation of graphitic material providing increasing sites for gas absorption. This is interesting to note as PXRD and IR data indicate a C_{60} fcc crystal structure despite the large surface area established by BET.

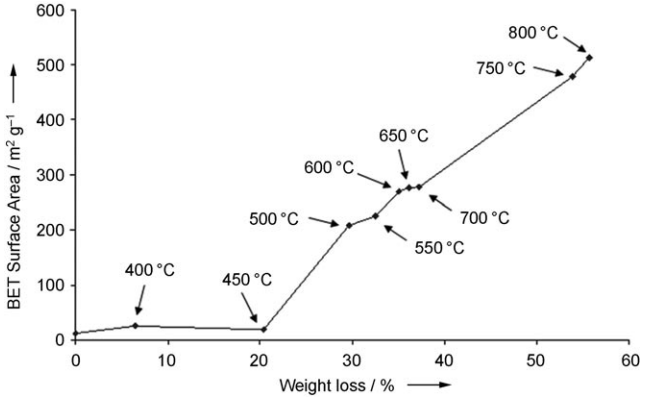

Figure 9. BET surface area against percent weight loss for as-synthesized and argon-annealed products, with associated annealing temperatures.

A study into the macroscopic electrical properties of the high temperature argon annealed analogues was carried out. The objective of this study was to confirm if high temperature argon annealing of the parent complex resulted in conductive material, which was inferred from the higher temperature SEM samples not being susceptible to charging

during imaging. The results for each sample were compared to that obtained for single crystals of pristine C_{60}, which at room temperature is known to be a highly insulating *n*-type material.[28] *I–V* curves and resistance values were obtained, with results shown for the 800 °C analogue (Figure 10). As

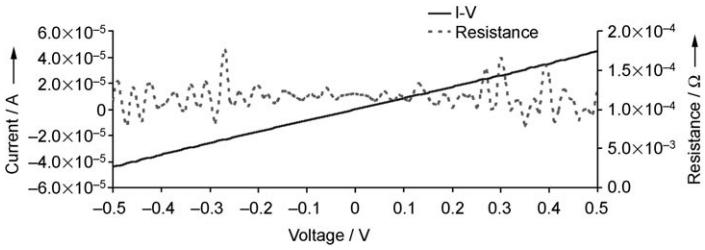

Figure 10. *I–V* and resistance curves for the analogue annealed under argon at 800 °C.

expected a non-ohmic conductance response was obtained for a single crystal of C_{60} at room temperature which is a known insulating material. Similar results were obtained for all the analogues annealed under argon until the annealing temperature of $\geq$650 °C was reached, whereby the materials exhibited an ohmic conductance response. This is clearly seen for the 800 °C analogue where a linear *I–V* curve and a relatively stable resistance value are produced through the voltage sweep (Figure 10). The bulk material resistance values obtained for the 800 °C analogues were about 1200Ω. These results reinforce the assumption that the material formed under an argon atmosphere at annealing temperatures of $\geq$650 °C forms a conductive material, the conductivity of which is ascribed to the formation of graphitic material, as discussed below.

Further experiments were carried out to assess the high temperature annealed samples to indicate a probable cause of the change in electrical behavior at specific temperatures. Dispersive Raman spectroscopy was undertaken on the range of high-temperature analogues and the as-synthesized product. The Raman spectrum of the as-synthesized product was similar to that of pure C_{60}. In contrast, the high temperature annealed material gave additional Raman lines (Figure 11), notably around 1580 cm^{-1} and 1330 cm^{-1}. These peaks correspond to the so-called G (graphite) and D (diamond) bands, respectively, and are in agreement with literature values.[29] The G band relates to the graphitic E_{2g} symmetry mode and reflects the structural integrity of the sp^2-hybridized carbon atoms of the graphitic material. While, the D band, or diamond band, indicates disordered sp^2-hybridized carbon atoms within the sample.

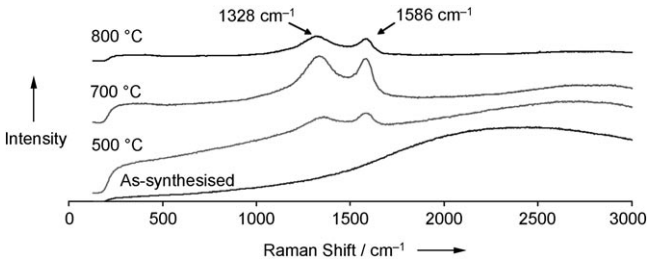

Figure 11. Raman spectra of the high-temperature analogues and as-synthesized product.

It is apparent that graphitic material is being formed in the annealing process. However, it is interesting to note that only the high-temperature annealed samples ($\geq$650 °C) exhibited conductive behavior, indicated by electrical resistance measurements. With the analysis of the G to D intensity ratios it is evident that a switch in the G to D ratio to less than one occurs when the material becomes conductive. This could either be due to the formation of more disordered carbon atoms at the higher temperatures or simply an increased coating is being formed fully encapsulating the fibers. In this context we note that the conducting material results in little dissolution of fullerene C_{60} in the presence of toluene. We conclude that at the higher temperatures ($\geq$ 650 °C) a graphitic material (not graphite itself), such as activated charcoal, encapsulates the remaining C_{60} fiber and forms a conductive sheath around a central core. The remaining presence of a C_{60} core is inferred from typical IR absorbance peaks attributed to C_{60}.

Conclusion

The results demonstrate the formation of C_{60} nanoarrays that form bundles of nanofibers based on complexation of C_{60} and *p*-*t*Bu-calix[5]arene from toluene in a quantitative yield. A grinding/sonication method for obtaining the complex has also been established, and complex formation is possible from crude fullerene soot. Annealing under an inert atmosphere demonstrates the use of this complex as a precursor in preparing exclusively carbon-based material, which can be conducting. The ensuing large surface area has implications for the development of catalyst support frameworks, hydrogen and other gas storage material architecture, and device technology.

Experimental Section

Synthesis of (C_{60})∩(*p*-*t*Bu-calix[5]arene): On dissolution of C_{60} (40.7 mg, 5.65×10^{-2} mmol, BuckyUSA 99 %) in toluene (40 mL), 13 molar equivalents of *p*-*t*Bu-calix[5]arene (596.3 mg, 0.7351 mmol) were added. Gravity filtration, followed by a wash with hexane (3×2 mL), afforded a light brown/golden solid (48.7 mg, 3.18×10^{-2} mmol), which was dried under vacuum (56 % yield, elemental analysis (%) calcd: C 90.17, H 5.22; found: C 90.14, H 5.28).

Transmission electron microscopy (TEM) was performed on a JEOL 3000F FEGTEM operating at 200 kV; sample preparation involved forming a liquid suspension of the complex in hexane and then putting a drop of the dispersion onto a holey carbon film supported by copper grids and air-dried. As-prepared samples and annealed analogues were directly examined on a Zeiss 1555 VP field emission scanning electron microscope; sample preparation involved the dispersion of material directly onto carbon tape on a standard aluminum stub.

Solid-state C^{13} CP-MAS spectra were measured on a Bruker ARX 300 MHz NMR spectrometer at a frequency of 75.468 MHz, a spin rate of 4 kHz, contact time of two milliseconds and relaxation delay of two seconds. Powder XRD patterns were obtained on a Siemens Diffractometer D500 by utilizing $Cu_{K\alpha}$ radiation ($\lambda = 0.154$ nm); sample preparation involved placing approximately 50 mg of material on a XRD sample holder, levelled with a glass microscope slide.

Thermogravimetric analysis (TGA) was performed on a TA Instruments SDT 2960 Simultaneous DSC-TGA in either air or argon (100 mL min^{-1}) with a temperature program of 3 °C min^{-1} for varied temperature ranges. For isothermal hold experiments a temperature program of 20 °C min^{-1} under argon (100 mL min^{-1}) with a 20 minute hold period at the programmed final temperature. Brunauer, Emmett, and Teller (BET) surface area measurements were measured by adsorption of N_2 at 77 K using a Micromeritics Tristar 3000; the sample was loaded in a quartz tube evacuated to 0.1 millibar and cooled with liquid nitrogen to 77 K. Nitrogen gas was incrementally released into the quartz tube for absorption measurements at different vapor pressures. Electrical resistance measurements were carried out on the samples using a micromanipulator coupled with a precision semiconductor parameter analyzer (Hewlett Packard, 4156 A). Dispersive Raman spectroscopy was performed with a Dilor Labram 1B Raman spectrometer instrument. The spectral range covered 127.38 to 3063.17 cm^{-1} using a grating of 600 lines per mm. The samples were mounted and analyzed on glass microscope slides.

Acknowledgements

The authors gratefully acknowledge the Australian Research Council for support of this work. We would like to acknowledge that electron microscopy was carried out using facilities at the Centre for Microscopy and Microanalysis/Biomedical Image and Analysis Facility, The University of Western Australia, which are supported by University, State, and Federal Government funding. We would also like to acknowledge Dr. Charlie Musca from the School of Electrical, Electronic, and Computer Engineering for assistance with the electrical measurements carried out on the samples.

[1] M. J. Ledoux, R. Vieira, C. Pham-Huu, N. Keller, *J. Catal.* **2003**, *216*, 333–342.
[2] M. Hara, T. Yoshida, A. Takagaki, T. Takata, J. N. Kondo, S. Hayashi, K. Domen, *Angew. Chem.* **2004**, *116*, 3015–3018; *Angew. Chem. Int. Ed.* **2004**, *43*, 2955–2958.
[3] A.-H. Lu, W. Schmidt, N. Matoussevitch, H. Bonnemann, B. Spliethoff, B. Tesche, E. Bill, W. Kiefer, F. Schuth, *Angew. Chem.* **2004**, *116*, 4403–4406; *Angew. Chem. Int. Ed.* **2004**, *43*, 4303–4306.
[4] N. Keller, G. Rebmann, E. Barraud, O. Zahraa, V. Keller, *Catal. Today* **2005**, *101*, 323–329.
[5] Y. Fangli, R. Hojin, *Nanotechnology* **2004**, *15*, S596-S602.
[6] F. Su, J. Zeng, Y. Yu, L. Lu, J. Y. Lee, X. S. Zhao, *Carbon* **2005**, *43*, 2366–2373.
[7] G. S. Chai, S. B. Yoon, J.-S. Yu, *Carbon* **2005**, *43*, 3028–3031.
[8] M. A. de la Casa-Lillo, B. C. Moore, D. Cazorla-Amoros, A. Linares-Solano, *Carbon* **2002**, *40*, 2489–2494.
[9] S. M. Saufi, A. F. Ismail, *Carbon* **2004**, *42*, 241–259.
[10] T. Yamamoto, A. Endo, T. Ohmori, M. Nakaiwa, *Carbon* **2004**, *42*, 1671–1676.
[11] L. Shi, X. Liu, H. Li, W. Niu, G. Xu, *Anal. Chem.* **2006**, *78*, 1345–1348.
[12] J. Kong, N. R. Franklin, C. Zhou, M. G. Chapline, S. Peng, K. Cho, H. Dailt, *Science* **2000**, *287*, 622–625.
[13] E. S. Snow, F. K. Perkins, E. J. Houser, B. S. C. , T. L. Reinecke, *Science* **2005**, *307*, 1942–1945.
[14] H. Xie, Q. Yang, X. Sun, J. Yang, Y. Huang, *Sens. Actuators B* **2006**, *113*, 887–891.
[15] G. D. Pantos, J.-L. Wietor, K. M. Sanders, *Angew. Chem.* **2007**, *119*, 2288–2290; *Angew. Chem. Int. Ed.* **2007**, *46*, 2238–2240.
[16] J. L. Atwood, G. A. Koutsantonis, C. L. Raston, *Nature* **1994**, *368*, 229–231.
[17] T. Suzuki, K. Nakashima, S. Shinkai, *Chem. Lett.* **1994**, *4*, 699–702.
[18] J. L. Atwood, L. J. Barbour, C. L. Raston, *Cryst. Growth Des.* **2002**, *2*, 3–6.
[19] M. Makha, M. J. Hardie, C. L. Raston, *Chem. Commun.* **2002**, *14*, 1446–1447.
[20] M. Makha, A. Purich, C. L. Raston, A. N. Sobolev, *Eur. J. Inorg. Chem.* **2006**, 507–517.
[21] J. L. Atwood, M. J. Barnes, M. G. Gardiner, C. L. Raston, *Chem. Commun.* **1996**, *12*, 1449–1450.
[22] J. L. Atwood, L. J. Barbour, M. W. Heaven, C. L. Raston, *Angew. Chem.* **2003**, *115*, 3376–3379; *Angew. Chem. Int. Ed.* **2003**, *42*, 3254–3257.
[23] T. Haino, M. Yanase, Y. Fukazawa, *Tetrahedron Lett.* **1997**, *38*, 3739–3742.
[24] M. Makha, J. J. McKinnon, A. N. Sobolev, M. A. Spackman, C. L. Raston, *Chem. Eur. J.* **2007**, DOI: 10.1002/chem.200601188.
[25] Accelrys, MS Visualizer, Accelrys Software, Inc., San Diego, **2006**.
[26] A. Datta, R. Y. Kelkar, M. Datta, *J. Mater. Sci. Lett.* **1994**, *13*, 996–999.
[27] R. Malhotra, D. C. Lorents, Y. K. Bae, C. H. Becker, D. S. Tse, L. E. Jusinski, E. D. Wachsman, in *Fullerenes: synthesis, properties, and chemistry of large carbon clusters* (Eds.: G. S. Hammond, V. J. Kuck), American Chemical Society, Washington, D. C., **1992**, pp. 127–139.
[28] R. Maruyama, *J. Appl. Phys.* **2003**, *94*, 6871–6874.
[29] F. Tuinstra, J. L. Koenig, *J. Chem. Phys.* **1970**, *53*, 1126–1130.

Received: March 1, 2007
Published online: May 29, 2007

